AGU PUBLICATIONS

Geophysical Research Letters

RESEARCH LETTER
10.1002/2016GL070869

L. Lin and Z. Wang contributed equally to this work and are the joint first authors.

Key Points:
- The increased rate of precipitation extremes with global mean surface warming depends on the compositions of radiative forcing
- The increased rate of precipitation extremes with warming caused by aerosol forcing is significantly larger than that caused by GHG forcing
- Aerosol forcing in the coming decades can have a critical role in inducing change in precipitation extremes

Correspondence to:
Z. Wang,
wangzl@camscma.cn

Citation:
Lin, L., Z. Wang, Y. Xu, and Q. Fu (2016), Sensitivity of precipitation extremes to radiative forcing of greenhouse gases and aerosols, *Geophys. Res. Lett.*, *43*, 9860–9868 doi:10.1002/2016GL070869.

Received 25 MAY 2016
Accepted 31 AUG 2016
Accepted article online 6 SEP 2016
Published online 19 SEP 2016

Sensitivity of precipitation extremes to radiative forcing of greenhouse gases and aerosols

Lei Lin[1,2,3], Zhili Wang[2], Yangyang Xu[4], and Qiang Fu[5]

[1]Department of Atmospheric Sciences, Sun Yat-sen University, Guangzhou, China, [2]State Key Laboratory of Severe Weather and Key Laboratory of Atmospheric Chemistry of CMA, Chinese Academy of Meteorological Sciences, Beijing, China, [3]College of Atmospheric Sciences, Lanzhou University, Lanzhou, China, [4]Department of Atmospheric Sciences, Texas A&M University, College Station, Texas, USA, [5]Department of Atmospheric Sciences, University of Washington, Seattle, Washington, USA

Abstract Greenhouse gases (GHGs) and aerosols are the two most important anthropogenic forcing agents in the 21st century. The expected declines of anthropogenic aerosols in the 21st century from present-day levels would cause an additional warming of the Earth's climate system, which would aggravate the climate extremes caused by GHG warming. We examine the increased rate of precipitation extremes with global mean surface warming in the 21st century caused by anthropogenic GHGs and aerosols, using an Earth system model ensemble simulation. Similar to mean precipitation, the increased rate of precipitation extremes caused by aerosol forcing is significantly larger than that caused by GHG forcing. The aerosol forcing in the coming decades can play a critical role in inducing change in precipitation extremes if a lower GHG emission pathway is adopted. Our results have implications for policy-making on climate adaptation to extreme precipitation events.

1. Introduction

The response of precipitation extremes to climate change is attracting attention because of the disastrous effects on human life and property, social economy, agriculture, and ecosystem [*Easterling et al*., 2000; *Knapp et al*., 2008; *Schiermeier*, 2011]. Observational analyses showed that precipitation extremes in many regions increased significantly during recent decades, in terms of both frequency and intensity [*Donat et al*., 2013]. It has also been shown that the warming caused by greenhouse gas (GHG) increases contributes significantly to the increase in precipitation extremes [*Min et al*., 2011; *Pall et al*., 2011].

The increase in precipitation extremes is expected to continue in the future [*Trenberth*, 1999; *O'Gorman*, 2012; *Kharin et al*., 2013]. The latest work by *Pendergrass et al*. [2015] indicated that the increased rate in precipitation extremes (i.e., the increase in precipitation extremes scaled by global mean surface warming) does not depend on emission scenarios, such as those in Representative Concentration Pathways (RCPs) [*Moss et al*., 2010]. This behavior of precipitation extremes is very different from global-mean precipitation, whose increased rate differs significantly across emission scenarios [*Pendergrass et al*., 2015]. This is because the increased rate of mean precipitation depends on the composition of forcing agents (e.g., the fraction of GHGs versus aerosols), and different emission scenarios have different compositions in forcing [*Andrews et al*., 2010; *Pendergrass et al*., 2015; *Lin et al*., 2016]. However, *Pendergrass et al*. [2015] have not investigated the increased rate of precipitation extremes caused by individual forcing agents.

GHGs and aerosols will continue to be the two most important anthropogenic forcing agents in the 21st century [*Myhre et al*., 2013]. The expected declines of anthropogenic aerosols in the 21st century from present-day levels would impose an additional warming on the Earth [*Rotstayn et al*., 2013; *Wang et al*., 2015; *Lin et al*., 2015], which will aggravate the climate extremes caused by GHGs-induced warming [*Xu et al*., 2015; *Wang et al*., 2016a]. Separating the contributions by different forcing agents to extreme precipitation increases under different emission scenarios would be beneficial to policy-making on climate mitigation and adaptation.

This study explores the rate of increase in precipitation extremes caused by anthropogenic GHGs and aerosols in the 21st century using an Earth system model ensemble simulation. Various indices that measure precipitation extremes including the one examined by *Pendergrass et al*. [2015] are considered. The relative contribution of GHGs and aerosols to the increase in precipitation extremes under both

RCP8.5 scenario (a nonmitigation scenario) [*Riahi et al*., 2007] and RCP4.5 scenario (a pathway of medium-low GHG emission) [*Clarke et al*., 2007] will also be examined. Section 2 describes the methodology, including model, model simulations, and precipitation extreme indices adopted in this work. Section 3 presents the results. The discussion and conclusions are given in sections 4 and 5, respectively.

2. Methodology

2.1. Global Climate Model

We used the Community Earth System Model (CESM1), a fully coupled global climate model [*Hurrell et al*., 2013]. The model has a 0.9° (latitude) × 1.25° (longitude) spatial resolution for the atmosphere and land components, and 1° × 1° spatial resolution for the ocean component. The three-mode modal aerosol model, which includes Aitken, accumulation, and coarse modes, has been implemented in the CESM1 [*Liu et al*., 2012]. The aerosol direct, semidirect, and indirect forcings for both liquid and ice phase clouds are included [*Morrison and Gettelman*, 2008; *Gettelman et al*., 2010; *Ghan et al*., 2012].

2.2. Model Experiments

The daily model outputs from three sets of CESM1 ensemble simulations were used: the RCP8.5 Large Ensemble (LE) [*Kay et al*., 2014], RCP8.5 with fixed aerosol Medium Ensemble (RCP8.5_FixA ME) [*Xu et al*., 2015], and RCP4.5 ME [*Sanderson et al*., 2015]. The RCP8.5 LE simulations consist of 30-member ensembles from 1920 to 2100 based on the RCP8.5 scenario. The same evolutions of GHG and aerosol forcings pertained in each member, but with slightly different atmospheric initial conditions. The RCP8.5_FixA ME simulations (2005–2100) are composed of 15-member ensembles that also adopt the forcing under the RCP8.5 scenario, but all emissions of aerosols and atmospheric oxidants are fixed at year 2005 levels. The RCP4.5 ME simulations, consisting of 15-member ensembles from 2005 to 2080, are similar to RCP8.5 ensemble simulations but follow the RCP4.5 scenario.

The changes in precipitation extremes over different time periods in the RCP8.5 or RCP4.5 scenarios are caused by changes in both GHGs and aerosols, while the changes in the RCP8.5_FixA scenario are only caused by GHGs. We could therefore obtain the sole effect of aerosols in RCP8.5 by subtracting the simulations in RCP8.5_FixA from the simulations in RCP8.5. Note that the reductions in aerosol emissions are similar for the RCP8.5 and RCP4.5 scenarios [*van Vuuren et al*., 2011].

2.3. Extreme Precipitation Indices

We examined four indices based on daily precipitation for each model grid cell, as described by the Expert Team for Climate Change Detection and Indices [*Zhang et al*., 2011], that included the monthly maximum 1 day precipitation (RX1day, thus 12 days in a year), the monthly maximum consecutive 5 day precipitation (RX5day, thus 60 days in a year), the total precipitation from the days with daily precipitation exceeding 95th percentile of daily rainfall distribution (R95p, about 18 days in a year), and the number of days with daily precipitation more than 10 mm (R10). RX1day and RX5day can be used as an indicator of flooding [*Lavers et al*., 2011]. R95p is the index of very wet days, and R10 is the number of heavy precipitation days. For the purpose of comparison, we also calculated the maximum daily precipitation in a year (RX1day_Annual), which is the index used by *Pendergrass et al*. [2015].

3. Results

We examine the changes in the globe- and land-averaged precipitation and precipitation extremes per degree of change in global mean surface temperature (i.e., the rate of change in these quantities). In deriving these rates, we first select the mean value of 1986–2005 as the reference and then calculate the decadal average of surface temperature, precipitation, and precipitation extremes in each of the subsequent decades (i.e., 2006–2015 and 2016–2025). Following *Pendergrass et al*. [2015], the rates of changes with surface warming are obtained by regressing the changes in precipitation and precipitation extremes to the global mean surface temperature changes. For consistency among various simulations, the data from 1986 to 2080 are analyzed. As an example, Figure 1 exhibits the scatterplot of changes in land-averaged precipitation and precipitation extremes versus global mean surface temperature changes due to GHG forcing and aerosol forcing from the RCP8.5 scenario, along with the linear fitting. Similar to the changes in mean precipitation,

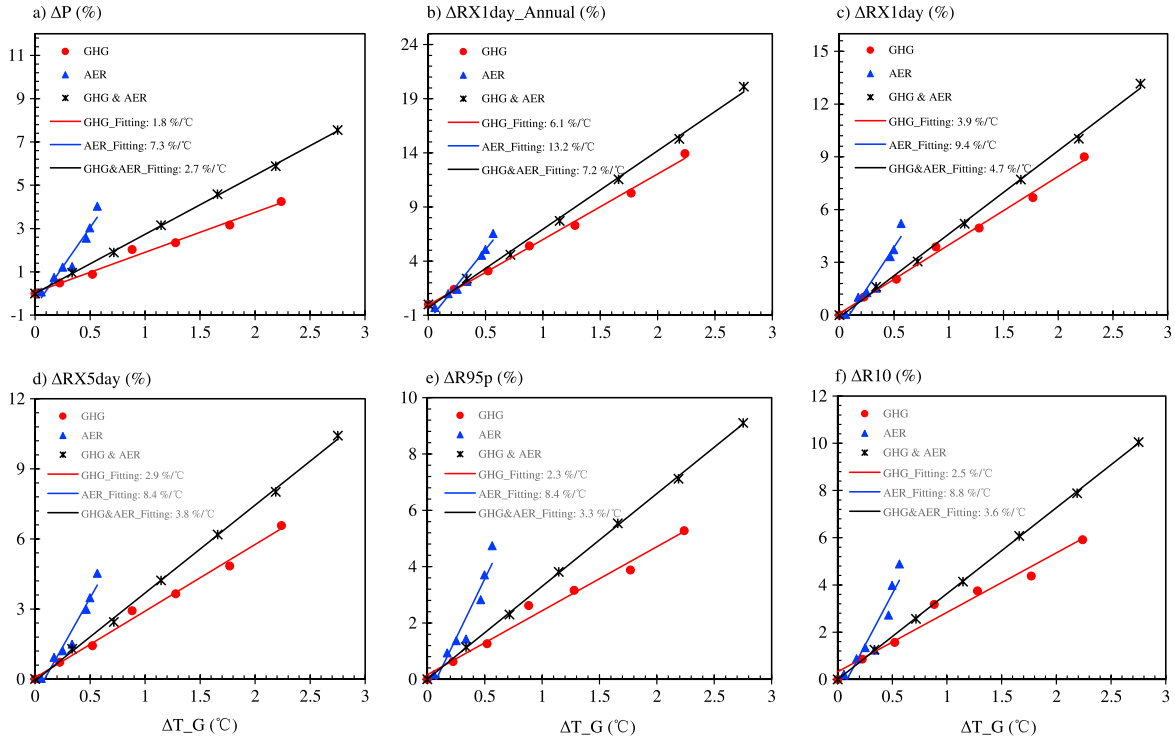

Figure 1. Scatterplot of changes in (a) land-averaged precipitation and (b–f) precipitation extremes (*y* axis) versus global mean surface temperature changes (*x* axis) because of GHG, aerosol (AER), and GHG and AER forcings from RCP8.5.

all the precipitation extremes show a linear increase with the surface warming caused by both aerosol forcing and GHG forcing (Figure 1). The slope of the linear fitting provides the estimate of increased rate.

Table 1 presents all derived rates of changes in mean precipitation and precipitation extremes caused by GHG and aerosol forcings from RCP8.5 over land and globe. The ratios of rates caused by aerosols and those caused by GHGs are also shown in Table 1. The alternative approach of using epoch differences gives similar results. Over land, the rates of increases in precipitation extremes caused by aerosol forcing are 2.2–3.7 times of those caused by GHG forcing, while the increased rate of mean precipitation caused by aerosol forcing is four times that of GHG forcing. The corresponding values are 1.8–2.4 for precipitation extremes and 2.8 for mean precipitation over the globe. However, the large uncertainties associated with the ratios suggest that the aerosol enhancements of the mean precipitation and precipitation extremes are statistically indistinguishable.

A stronger role of aerosols than GHGs in changing mean precipitation, especially over land, is expected. First, precipitation change is constrained by atmospheric net radiative cooling. Atmospheric heating resulting

Table 1. The Rates of Changes in Land- and Globe-Averaged Precipitation (P) and Precipitation Extremes with Global Mean Surface Temperature Increase Caused by GHG and Aerosol (AER) Forcing From RCP8.5 and their Ratios[a]

	Land			Globe		
	AER (% °C^{-1})	GHG (% °C^{-1})	Ratio (AER/GHG)	AER (% °C^{-1})	GHG (% °C^{-1})	Ratio (AER/GHG)
P	7.3 (4.42)	1.8 (0.73)	4.0 (4.09)	3.5 (0.90)	1.3 (0.13)	2.8 (0.85)
RX1day_Annual	13.2 (7.80)	6.1 (0.94)	2.2 (1.55)	11.7 (5.81)	5.5 (0.84)	2.1 (1.03)
RX1day	9.4 (6.65)	3.9 (0.88)	2.4 (2.22)	6.5 (3.05)	3.0 (0.40)	2.1 (0.85)
RX5day	8.4 (5.72)	2.9 (0.84)	2.9 (2.97)	4.7 (2.17)	2.1 (0.31)	2.3 (1.09)
R95p	8.4 (5.65)	2.3 (0.84)	3.7 (4.22)	4.1 (1.18)	1.7 (0.15)	2.4 (0.82)
R10	8.8 (6.02)	2.5 (1.02)	3.5 (4.17)	3.0 (0.86)	1.7 (0.20)	1.8 (0.59)

[a]All results are significant at the 99% confidence level from the *t* test. The values in parentheses are 2 standard deviations, presented for both the internal variability (ensemble variability) and least squares fitting uncertainty for AER and GHG columns, with the former dominating, whereas they are only due to the internal variability for ratio column.

from GHG increases suppresses the response of precipitation to warming through rapid adjustment as compared to scattering aerosols [e.g., *Wu et al*., 2013; *Allan et al*., 2014]. Moreover, a reduction of aerosols (both scattering and absorbing) can produce a positive radiative forcing at the top of the atmosphere but negative radiative forcing within the atmosphere compared to the present day [*Wang et al*., 2016b]. Such a vertical configuration of aerosol forcings induces a larger response of water cycle compared to GHGs; the latter leads to positive forcings both at the top of the atmosphere and within the atmospheric column [*Rotstayn et al*., 2013; *Pendergrass and Hartmann*, 2014a]. Second, aerosols can affect precipitation by altering cloud microphysical characteristics [*Myhre et al*., 2013]. Third, the spatial structure of aerosol forcing can alter the land/ocean partitioning and distribution of precipitation via dynamical responses to forcings [e.g., *Bollasina et al*., 2011; *Li et al*., 2015; *Wang et al*., 2016b].

Table 1 shows that the changes of aerosols lead to a larger rate of increase with warming not only in mean precipitation but also in precipitation extremes. However, the ratio of the change rate caused by aerosols versus that by GHGs for mean precipitation is larger than those ratios derived from precipitation extremes (Table 1). Note that the rates of change in precipitation and precipitation extremes resulting from individual forcing agents should not be sensitive to the emission scenario in use, although the individual rate is derived from the RCP8.5_FixA and RCP8.5 simulations.

One concern is that the difference in the increased rate of RCP8.5 and RCP8.5_FixA is caused by the "extreme mode" in the model resulting from the additional warming from aerosols, rather than from the aerosol forcing itself. The extreme mode is the temperature dependence of increased rate [*Pendergrass and Hartmann,* 2014b], so the extra warming from the aerosol forcing in RCP8.5 would give a nonlinear response in precipitation. Because the extreme modes mainly originate from tropical ocean, we test it by calculating all the metrics but only for extratropics land. We find that the ratio of aerosol (AER)/GHG is still significantly larger than 1 for all the metrics (not shown), indicating that the nonlinearity issue is not likely the main contributor.

Since the role of aerosols appears to be stronger for land- and globe-averaged precipitation metrics, it is worth investigating the spatial distribution of the rates of change in mean precipitation and precipitation extremes with warming due to GHGs and aerosols. The spatial patterns of the increased rates of all precipitation extremes are roughly consistent for the same forcing and are also similar to those in mean precipitation (Figure 2). The rates of changes in precipitation extremes caused by both forcing agents are positive over most of the globe, but the magnitudes due to aerosols are markedly larger. In particular, the increased rates in precipitation extremes caused by aerosols are 10 times of those attributable to GHGs in eastern China, Southeast Asia, northwestern Europe, and central South and North America, where the aerosol loadings are high. This is primarily because of the dynamical response to aerosol forcing. For example, *Zhang and Li* [2016] showed that the decrease of land-ocean thermal contrast and rainfall over land monsoon regions were dominated by the effect of aerosol forcing during the historical boreal summer period, attributing to more localized distribution of anthropogenic aerosols over the lands compared with the well-mixed GHGs. Thus, the reductions in aerosol emissions can enhance the local monsoon circulations over those regions, bringing more moisture from the oceans toward the land and leading to more precipitation over land [*Wang et al*., 2016b]. *Li et al*. [2015] also indicated that the summer drying trend over the Asian monsoon region during the historical period was dominated by the change in circulation caused by the aerosol forcing in the Coupled Model Intercomparison Program phase 5 (CMIP5) all-forcing simulations, and air pollution control policies would beneficially increase precipitation in the future. However, the rates of changes in precipitation extremes resulting from both forcings are opposite in northern South America, southern North America, and central Australia, with the largest absolute difference more than a factor of 10.

Note that the absolute value of the future change in precipitation extremes depends not only on the rate of change with warming but also on the underlying surface warming caused by forcing agents. Figure 3 presents the changes in surface temperature, precipitation, and precipitation extremes over time caused by different forcings for the RCP8.5 and RCP4.5 scenarios. The RCP8.5 is characterized by significantly increasing GHG emissions with time. We can see that although the increase in surface temperature caused by aerosols is much lower than that by GHGs, the increases in mean precipitation and precipitation extremes by both forcings are comparable over the coming decades under this scenario.

It is assumed in this paper that the changes in surface temperature caused by aerosols in the RCP4.5 scenario are same as those in the RCP8.5 scenario, because of the similar reduction in aerosol emissions under both

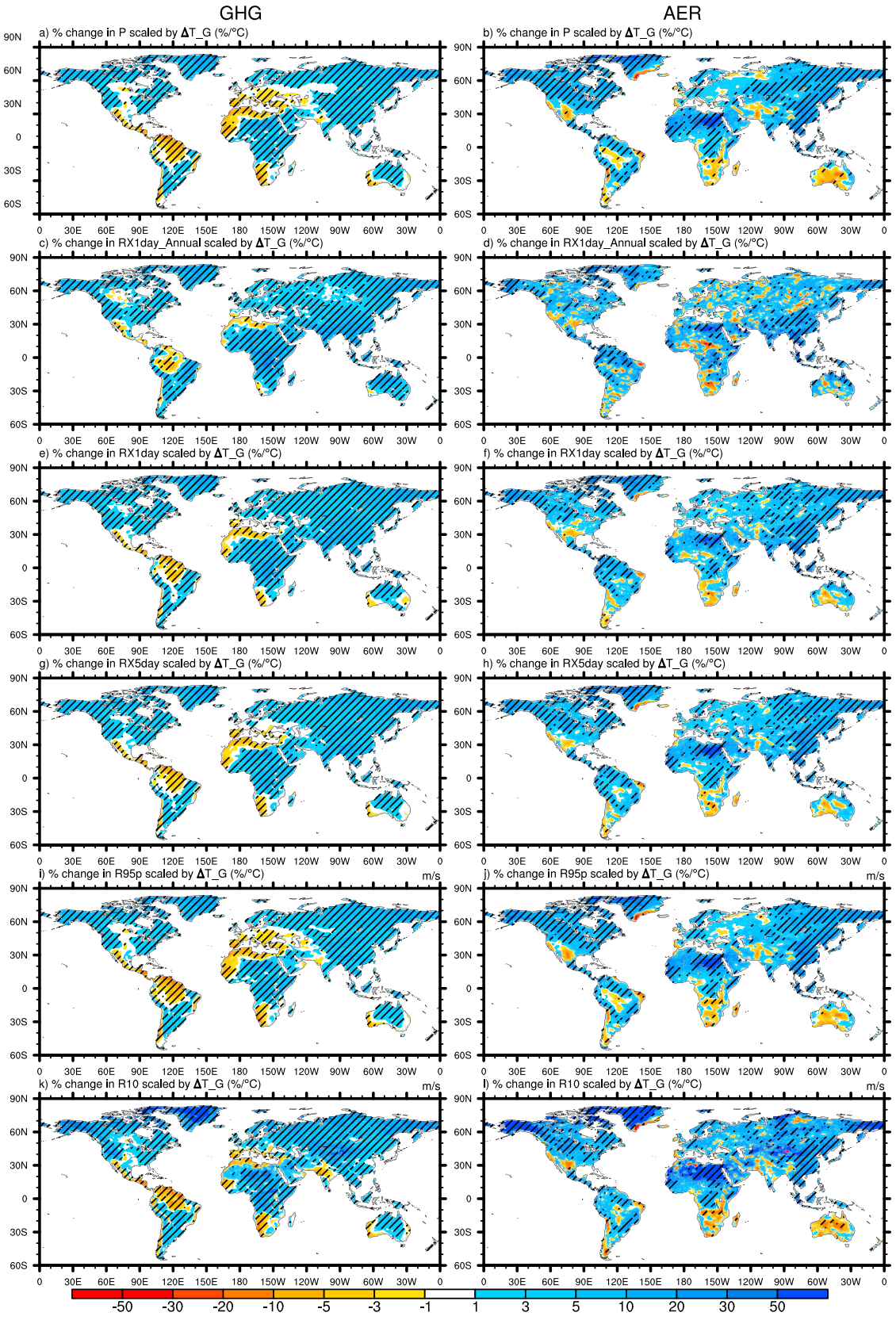

Figure 2. Spatial distributions of the rates of changes in (a and b) precipitation and (c–l) precipitation extremes with global mean surface temperature increases caused by (left column) GHG forcing and (right column) aerosol (AER) forcing (right). The dots represent significance at ≥95% confidence level from the *t* test.

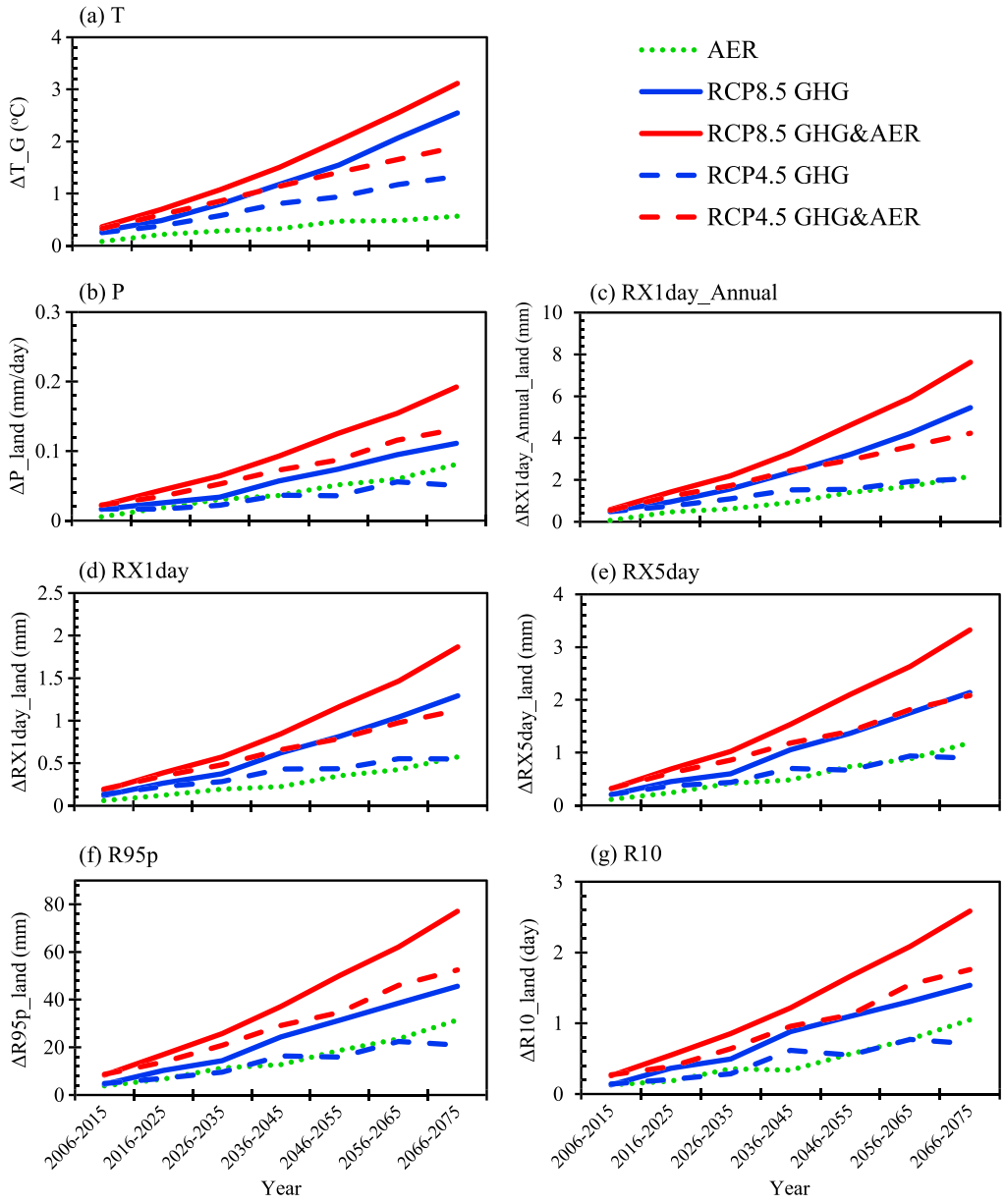

Figure 3. Time series of changes in every decade for global mean surface temperature (*T*), land-averaged precipitation (*P*), and precipitation extremes resulting from GHG, aerosol (AER), and GHG and AER forcing under the RCP8.5 and RCP4.5 scenarios relative to the 1986–2005 reference, respectively.

scenarios [*van Vuuren et al*., 2011, also see supplement figure of *Xu et al*., 2015]. As in Figure 3, the increases in mean precipitation and precipitation extremes from aerosols are comparable to, or even larger than, those from GHGs in RCP4.5. This suggests that aerosol forcing can play an important role in the future change of precipitation extremes if a lower emission pathway of GHGs (RCP4.5 as opposed to RCP8.5) is adopted.

4. Discussion

We have shown that the increased rate of precipitation extremes is significantly different in response to aerosol forcing and GHG forcing. This result differs from what is implied by *Pendergrass et al*. [2015] in terms of the CMIP5 multimodel ensemble simulations under the four RCP scenarios. *Pendergrass et al*. [2015] indicated that future increases in precipitation extremes, unlike the mean precipitations, depend only on the magnitude of surface temperature increase, not on the emission scenarios, which may have a different composition of forcing.

Table 2. Same as Table 1 but Showing the Rates of Changes Resulting From Combining GHG and Aerosol Forcing From RCP8.5, RCP4.5, and RCP2.6

	Land			Globe		
	RCP8.5 (% °C^{-1})	RCP4.5 (% °C^{-1})	RCP2.6 (% °C^{-1})	RCP8.5 (% °C^{-1})	RCP4.5 (% °C^{-1})	RCP2.6 (% °C^{-1})
P	2.7 (0.68)	3.1 (0.94)	4.3 (1.39)	1.6 (0.11)	2.0 (0.20)	2.9 (0.46)
RX1day_Annual	7.2 (0.91)	6.6 (1.43)	7.1 (1.38)	6.5 (0.95)	5.2 (1.06)	5.4 (1.53)
RX1day	4.7 (0.78)	4.6 (1.33)	5.3 (0.97)	3.6 (0.41)	3.2 (0.57)	3.6 (0.57)
RX5day	3.8 (0.69)	3.9 (1.09)	4.9 (1.26)	2.5 (0.24)	2.4 (0.42)	3.1 (0.62)
R95p	3.3 (0.81)	3.8 (1.09)	5.0 (1.65)	2.1 (0.16)	2.5 (0.28)	3.5 (0.55)
R10	3.6 (0.94)	4.2 (1.41)	5.4 (2.48)	1.9 (0.21)	2.6 (0.21)	3.5 (0.54)

The first point of *Pendergrass et al*. [2015] can be seen in the top row of our Table 2 for global annual mean precipitation. The increased rate from RCP2.6 is significantly larger than that from RCP4.5 and RCP8.5, because of a larger fractional contribution of aerosol forcing to total forcing in RCP2.6 (i.e., the same aerosol forcing with smaller GHG forcing) [*van Vuuren et al*., 2011]. The physical explanation is that the rate of change in mean precipitation is largely bounded to atmospheric radiative cooling and the change in atmospheric radiative cooling differs among forcing agents [*Pendergrass and Hartmann*, 2014a; *Pendergrass et al*., 2015]. Since aerosol forcing leads to a larger normalized change in mean precipitation and precipitation extremes in the RCP2.6 scenario than in the RCP4.5 and RCP8.5 scenarios, it is expected that the increased rate of those metrics from the RCP2.6 should be larger. Table 2 shows that the increased rates of mean precipitation, RX5day, R95p, and R10 from RCP2.6 are indeed larger than those from RCP4.5 and RCP8.5.

The second point of *Pendergrass et al*. [2015] is that for very extreme precipitation (RX1day_Annual), which usually forms under intense convergence conditions with sufficient moisture supply, the atmospheric energy argument no longer holds; i.e., there are no significant differences in the increased rates of RX1day_Annual across various scenarios. This is also consistent with our analysis that the change rates in those "very extreme" indices (RX1day_Annual and RX1day) are not significantly different among different scenarios (Table 2). The high variance is because those daily-based extreme indices are strongly impacted by the internal variability. There is yet a further complication in *Pendergrass et al*. [2015]. The diversity of the results across the CMIP5 models and the different resolutions of data used (2.5° × 2.5° in *Pendergrass et al*. [2015]) can also contribute to the inconsistent results between *Pendergrass et al*. [2015] and this study. In addition, the insignificant difference in change rates between from RCP8.5 and RCP4.5 could be partly because the GHG radiative forcing dominates while the evolution of aerosol emissions is similar in both scenarios [*van Vuuren et al*., 2011].

Nevertheless, what we have analyzed here is the dependence of scenarios (the difference of response to GHGs and aerosols) across different extreme precipitation definitions. Those loosely defined extreme indices may be more relevant to flooding and other hazards [*Lavers et al*., 2011]. Under those *less* extreme conditions, the atmospheric energy argument holds better.

5. Conclusions

We have explored the rates of changes in precipitation extremes with global mean surface temperature increase caused by GHG forcing and aerosol forcing in the 21st century by using the CESM1 ensemble simulations. We find that the change of precipitation extremes per degree of surface warming, much like what is seen for mean precipitation, markedly depends on the composition of radiative forcing in different emissions scenarios. The aerosol forcing leads to a larger increased rate than GHG forcing by a factor of 2 to 4 for various precipitation extremes indices, with a large uncertainty. The change rates of precipitation extremes due to both forcings are positive over most of the globe, but the values attributable to aerosols are 10 times those of GHGs in eastern China, Southeast Asia, northwestern Europe, and Central South and North America.

Reducing aerosol emissions will be an inevitable trend driven by benefits to human health, as is shown in RCPs. The aerosol forcing can play an important role in the future change of precipitation extremes if a lower emission pathway of GHGs is adopted. Therefore, the impact of aerosols on precipitation extremes calls for greater attention in future research. Note that our results are based on one climate model, although large ensemble simulations are used. Since the responses of climate to aerosol and GHG forcings can be different

among different models [*Lamarque et al*., 2013], it will be very useful to perform similar analyses using other global climate models, such as the recently available data set described by *Samset et al*. [2016] to check the robustness of our results.

Acknowledgments
This study was supported by the National Key Project of MOST (2016YFC0203306), the Fund for Creative Research Groups of National Natural Science Foundation of China (41321001), the National Natural Science Foundation of China (41575139, 41305025, 41330527, and 41575006) and Jiangsu Collaborative Innovation Center for Climate Change. Y.X. was supported by a postdoctoral fellowship from the Advanced Study Program of NCAR and the Regional and Global Climate Modeling Program of the U.S. Department of Energy's Office of Science, Cooperative Agreement DE-FC02-97ER62402. Computing resources (ark:/85065/d7wd3xhc) were provided by the Climate Simulation Laboratory at NCAR's Computational and Information Systems Laboratory, sponsored by the National Science Foundation (NSF) and other agencies. NCAR is funded by the NSF. For data requests, please contact the corresponding author (wangzl@camscma.cn).

References

Allan, R. P., C. Liu, M. Zahn, D. A. Lavers, E. Koukouvagias, and A. Bodas-Salcedo (2014), Physically consistent responses of the global atmospheric hydrological cycle in models and observations, *Surv. Geophys.*, *35*, 533–552.

Andrews, T., P. M. Forster, O. Boucher, N. Bellouin, and A. Jones (2010), Precipitation, radiative forcing and global temperature change, *Geophys. Res. Lett.*, *37*, L14701, doi:10.1029/2010GL043991.

Bollasina, M., Y. Ming, and V. Ramaswamy (2011), Anthropogenic aerosols and the weakening of the South Asian summer monsoon, *Science*, *28*, 502–505.

Clarke, L., J. Edmonds, H. Jacoby, H. Pitcher, J. Reilly, and R. Richels (2007), Scenarios of greenhouse gas emissions and atmospheric concentrations. Sub-report 2.1A of Synthesis and Assessment Product 2.1 by the U.S. Climate Change Science Program and the Subcommittee on Global Change Research, Dep. of Energy, Office of Biol. & Environ. Res., Washington, 7 DC, 154 pp.

Donat, M. G., et al. (2013), Updated analyses of temperature and precipitation extreme indices since the beginning of the twentieth century: The HadEX2 dataset, *J. Geophys. Res. Atmos.*, *118*, 2098–2118, doi:10.1029/2012JD018606.

Easterling, D. R., G. A. Meehl, C. Parmesan, S. A. Changnon, T. R. Karl, and L. O. Mearns (2000), Climate extremes: Observations, modeling, and impacts, *Science*, *289*(5487), 2068–2074, doi:10.1126/science.289.5487.2068.

Gettelman, A., X. Liu, S. J. Ghan, H. Morrison, S. Park, A. J. Conley, S. A. Klein, J. Boyle, D. L. Mitchell, and J.-L. F. Li (2010), Global simulations of ice nucleation and ice supersaturation with an improved cloud scheme in the community atmosphere model, *J. Geophys. Res.*, *115*, D18216, doi:10.1029/2009JD013797.

Ghan, S. J., X. Liu, R. C. Easter, R. Zaveri, P. J. Rasch, J.-H. Yoon, and B. Eaton (2012), Toward a minimal representation of aerosols in climate models: Comparative decomposition of aerosol direct, semi-direct and indirect radiative forcing, *J. Clim.*, *25*, 6461–6476, doi:10.1175/JCLI-D-11-00650.1.

Hurrell, J. W., et al. (2013), The Community Earth System Model: A framework for collaborative research, *Bull. Am. Meteorol. Soc.*, *94*, 1339–1360, doi:10.1175/BAMS-D-12-00121.1.

Kay, J. E., et al. (2014), The Community Earth System Model (CESM1) large ensemble project: A community resource for studying climate change in the presence of internal climate variability, *Bull. Am. Meteorol. Soc.*, *96*, 1333–1349, doi:10.1175/BAMS-D-13-00255.1.

Kharin, V. V., F. W. Zwiers, X. Zhang, and M. Wehner (2013), Changes in temperature and precipitation extremes in the CMIP5 ensemble, *Clim. Change*, *119*, 345–357, doi:10.1007/s10584-013-0705-8.

Knapp, A. K., et al. (2008), Consequences of more extreme precipitation regimes for terrestrial ecosystems, *BioScience*, *58*, 811–821, doi:10.1641/B580908.

Lamarque, J.-F., et al. (2013), The Atmospheric Chemistry and Climate Model Intercomparison Project (ACCMIP): Overview and description of models, simulations and climate diagnostics, *Geosci. Model Dev.*, *6*, 179–206, doi:10.5194/gmd-6-179-2013.

Lavers, D. A., R. P. Allan, E. F. Wood, G. Villarini, D. J. Brayshaw, and A. J. Wade (2011), Winter floods in Britain are connected to atmospheric rivers, *Geophys. Res. Lett.*, *38*, L23803, doi:10.1029/2011GL049783.

Li, X., M. Ting, C. Li, and N. Henderson (2015), Mechanisms of Asian summer monsoon changes in response to anthropogenic forcing in CMIP5 models, *J. Clim.*, *28*, 4107–4125.

Lin, L., A. Gettelman, Q. Fu, and Y. Xu (2015), Simulated differences in 21st century aridity due to different scenarios of greenhouse gases and aerosols, *Clim. Change*, doi:10.1007/s10584-016-1615-3.

Lin, L., A. Gettelman, Y. Xu, and Q. Fu (2016), Simulated responses of terrestrial aridity to black carbon and sulfate aerosols, *J. Geophys. Res. Atmos.*, *121*, 785–794, doi:10.1002/2015JD024100.

Liu, X., et al. (2012), Towards a minimal representation of aerosol direct and indirect effects: Model description and evaluation, *Geosci. Model Dev.*, *5*, 709–735, doi:10.5194/gmd-4-709-2012.

Min, S.-K., X. Zhang, F. W. Zwiers, and G. C. Hegerl (2011), Human contribution to more-intense precipitation extremes, *Nature*, *470*, 378–381, doi:10.1038/nature09763.

Morrison, H., and A. Gettelman (2008), A new two-moment bulk stratiform cloud microphysics scheme in the community atmosphere model, version 3 (CAM3). Part I: Description and numerical tests, *J. Clim.*, *21*, 3642–3659.

Moss, R. H., et al. (2010), The next generation of scenarios for climate change research and assessment, *Nature*, *463*, 747–756, doi:10.1038/nature08823.

Myhre, G., et al. (2013), Anthropogenic and natural radiative forcing, in *Climate Change 2013: The Physical Science Basis. Contribution of Working Group I to the Fifth Assessment Report of the Intergovernmental Panel on Climate Change*, edited by T. F. Stocker et al., pp. 659–740 , Cambridge Univ. Press, Cambridge, U. K., and New York.

O'Gorman, P. A. (2012), Sensitivity of tropical precipitation extremes to climate change, *Nat. Geosci.*, *5*, 697–700, doi:10.1038/ngeo1568.

Pall, P., T. Aina, D. A. Stone, P. A. Stott, T. Nozawa, A. G. J. Hilberts, D. Lohmann, and M. R. Allen (2011), Anthropogenic greenhouse gas contribution to flood risk in England and Wales in autumn 2000, *Nature*, *470*, 382–385, doi:10.1038/nature09762.

Pendergrass, A. G., and D. L. Hartmann (2014a), The atmospheric energy constraint on global-mean precipitation change, *J. Clim.*, *27*(2), 757–768, doi:10.1175/JCLI-D-13-00163.1.

Pendergrass, A. G., and D. L. Hartmann (2014b), Changes in the distribution of rain frequency and intensity in response to global warming*, *J. Clim.*, *27*(22), 8372–8383.

Pendergrass, A. G., F. Lehner, B. M. Sanderson, and Y. Xu (2015), Does extreme precipitation intensity depend on the emissions scenario? *Geophys. Res. Lett.*, *42*, 8767–8774, doi:10.1002/2015GL065854.

Riahi, K., A. Gruebler, and N. Nakicenovic (2007), Scenarios of long-term socio-economic and environmental development under climate stabilization, *Technol. Forecast. Soc. Change*, *74*(7), 887–935.

Rotstayn, L. D., M. A. Collier, A. Chrastansky, S. J. Jeffrey, and J.-J. Luo (2013), Projected effects of declining aerosols in RCP4.5: Unmasking global warming? *Atmos. Chem. Phys.*, *13*, 10,883–10,905, doi:10.5194/acp-13-10883-2013.

Samset, B. H., et al. (2016), Fast and slow precipitation responses to individual climate forcers: A PDRMIP multimodel study, *Geophys. Res. Lett.*, *43*, 2782–2791, doi:10.1002/2016GL068064.

Sanderson, B. M., C. Tebaldi, R. Knutti, and K. W. Oleson (2015), A new large CESM initial condition ensemble to assess avoided impacts in a climate mitigation scenario, *Clim. Change*, doi:10.1007/s10584-015-1567-z.
Schiermeier, Q. (2011), Increased flood risk linked to global warming, *Nature*, *470*, 316, doi:10.1038/470316a.
Trenberth, K. E. (1999), Conceptual framework for changes of extremes of the hydrological cycle with climate change, *Clim. Change*, *42*, 327–339.
van Vuuren, D. P., et al. (2011), The representative concentration pathways: An overview, *Clim. Change*, *109*, 5–31.
Wang, Z., H. Zhang, and X. Zhang (2015), Simultaneous reductions in emissions of black carbon and co-emitted species will weaken the aerosol net cooling effect, *Atmos. Chem. Phys.*, *15*, 3671–3685, doi:10.5194/acp-15-3671-2015.
Wang, Z., L. Lin, M. Yang, and Y. Xu (2016a), The effect of future reduction in aerosol emissions on climate extremes in China, *Clim. Dyn.*, doi:10.1007/s00382-016-3003-0.
Wang, Z., H. Zhang, and X. Y. Zhang (2016b), Projected response of East Asian summer monsoon system to future reductions in emissions of anthropogenic aerosols and their precursors, *Clim. Dyn.*, *47*, 1455–1468, doi:10.1007/s00382-015-2912-7.
Wu, P., N. Christidis, and P. Stott (2013), Anthropogenic impact on Earth's hydrological cycle, *Nat. Clim. Change*, *3*, 807–810.
Xu, Y., J.-F. Lamarque, and B. Sanderson (2015), The importance of aerosol scenarios in projections of future heat extremes, *Clim. Change*, doi:10.1007/s10584-015-1565-1.
Zhang, L., and T. Li (2016), Relative roles of anthropogenic aerosols and greenhouse gases in land and oceanic monsoon changes during past 156 years in CMIP5 models, *Geophys. Res. Lett.*, *43*, 5295–5301, doi:10.1002/2016GL069282.
Zhang, X., L. Alexander, G. C. Hegerl, P. Jones, A. K. Tank, T. C. Peterson, B. Trewin, and F. W. Zwiers (2011), Indices for monitoring changes in extremes based on daily temperature and precipitation data, *WIREs Clim. Change*, *2*, 851–870, doi:10.1002/wcc.147.